京 都 大 学 防 災 研 究 所 年 報　第47号 C 平成16年3月
Annuals of Disas. Prev. Res. Inst., Kyoto Univ., No. 47 C, 2004

Assessment of Landslide Risk during Earthquake/Rainfall on Urban Areas

Kyoji SASSA, Gonghui WANG, Hiroshi FUKUOKA

Synopsis

This paper introduced some recent landslides triggered by earthquake or rainfall on urban areas in Japan. These landslides include: 1) a landslide in a filled slope of 20 degrees on Nikawa area with 34 fatalities, which were triggered by the 1995 Hyogoken-Nanbu earthquake; 2) a landslide triggered by the 2003 Sanriku-Minami Earthquake on Tsukidate area, northwest of Sendai, Miyagi Prefecture; 3) a landslide triggered by the 2003 heavy rainfall on Minamata city, Kumamoto Prefecture. Their mechanisms were examined by using a multirole undrained ring shear apparatus. The investigation results showed that sliding surface liquefaction (Sassa 1996) played a key role on the triggering of these catastrophic landslides. Through these case studies, a method for the assessment of landslide risk on urban areas during earthquakes was proposed with the consideration of sliding surface liquefaction. This method was used for Nikawa slope area and a densely populated urban area near Tokyo. Detailed geological survey and laboratory ring shear simulation tests for Nikawa slope area presented the potential sliding surface as well as the potential soil layer where the sliding surface liquefaction behavior could be triggered, provided another earthquake would attack this area in the same scale as the 1995 Hyogoken-Nanbu earthquake. It is made clear that how to reduce the buildup of high pore-water pressure during earthquake shaking is essential in preventing the slope from sliding surface liquefaction failure, and then prevention measures were proposed correspondingly. Detailed airborne-laser-scanner-based micro-contour mapping, geological survey as well as results of undrained cyclic ring shear tests for the urban area near Tokyo revealed that this area is also facing the risk of rapid long traveling landslides during earthquakes.

Keywords: Landslide; Earthquake; Rainfall; Liquefaction; Risk assessment; Urban area

1. Introduction

Recent urban development is increasing the risk of landslides not only on mountainous areas, but also on rather flat areas. Japan is one of the countries having high landslide hazard susceptibility due to the limited flat area and its high population density. Recent worldwide population growth and rapid regional development are making a similar condition and landslide risk in many countries, especially those in Asia, Pacific and Latin America. The 1995 Hyogoken-Nanbu earthquake occurred in the driest season of January after the historically driest year of 1994 in Kansai area, Japan. Therefore, landslide disasters were limited comparing to damages to buildings, bridges, railways, highways and other manmade structures directly by the earthquake. However, the urban development magnified the risk of landslide disasters. One rapid landslide, which occurred on the Nikawa area (thereinafter termed as Nikawa landslide) destroyed 11 houses and killed 34 persons.

On May 2003, an earthquake (Sanriku-Minami) with a moment magnitude of 7.0 occurred in northern Japan. Due to this earthquake, a landslide was triggered on Tsukidate area, northwest of Sendai city. Compared to Nikawa landslide, Tsukidate landslide did not cause casualties fortunately. Nevertheless, the displaced landslide mass originated from a gentle slope with the inclination of sliding surface being about 14 degrees, and travelled a long distance, and finally deposited on a horizontal rice paddy.

Many landslides had also been triggered by rainfall recently in Japan on urban areas, such as the 1997 Harihara landslide in Izumi city, Kagosima Prefecture, the 1998 Taiyo-no-kuni landslide, Fukushima Prefec-ture, the 1999 landslides in Hiroshima city, causing great loss in both lives and properties. More recently, a landslide triggered by the heavy rainfall in Minamata city, Kumamoto Prefecture, destroyed 15 houses, killed 15 and injured an additional 6 people.

The Japanese Government has done works to prevent those landslides or slopes on, 1) moving or previously moved slopes, 2) slopes steeper than 30 degrees. In Fact, most landslides occurred as reactivation of previous landslides or in steep slopes as the first time landslides. Extensive landslide prevention works have been done for those dangerous slopes and they are very effective and the number of fatalities caused by landslides per year decreased significantly. However, as mentioned above, landslides were still causing great disasters. To prevent/mitigate landslide disasters on urban areas, it is necessary to have a better assessment of the landslide risk during earthquake or rainfall. Therefore, the mechanisms of these above-mentioned landslides were examined by performing a series of ring shear tests. A landslide risk assessment method for urban areas was proposed, and applied to two urban areas in Japan for the landslide prevention plan.

2. Recent Earthquake-induced Urban Landslide Disasters in Japan

2.1 Nikawa Landslide triggered by the 1995 Hyogoken-Nanbu earthquake

At the Hyogoken-Nanbu earthquake, many landslides were triggered in the metropolitan areas between Kobe and Osaka. Among them the largest landslide disaster was the Nikawa landslide, which killed all 34 residents sleeping in 11 houses below the slope. The volume of this landslide was 110,000 ~120,000 m^3, and the moving distance was about 175 m (Sassa et al. 1996). No recorded data concerning the sliding speed was available. However, it is believed that it was a rapid landslide, since no one evacuated from the destroyed houses and all 34 residents were killed. The locations of Nikawa and other two landslides introduced in this paper are presented in Fig. 1. Fig. 2 is a photograph showing the whole area of the Nikawa landslide, and Fig. 3 shows its geological section. Soon after the landslide hazard, 28 borings were executed and ground water table were monitored inside/outside the landslide area. The ground water surface existed in 6-7 m in depth, and the sliding surface was formed in 14 m deep (maximum) inside the embankment of Osaka group formation (limnic and marine deposits of granitic sands and clays in Pliocene to Middle Pleistocene). Therefore, the sliding surface was saturated. The slope was not steep, because the slope angle was about 20 degrees. The apparent friction angle that was calculated from the line connecting the top of initial landslide to the toe of deposition was 9.6 ~11.4 degrees, showing high mobility.

The Nikawa landslide and its mechanism were reported by Sassa (1996), using the undrained dynamic loading ring shear apparatus of DPRI-3. The test was performed in 0.1 Hz of sine curve. Recently a series of undrained ring shear apparatuses (DPRI-4, 5, 6, and 7) was developed and improved in DPRI, Kyoto University. These ring shear apparatus enable the application of cyclic loading in high frequency (3~5 Hz), and the late three ones enable simulating the seismic loadings using real recorded seismic wave during earthquakes. In 1997, we tried to simulate the Nikawa landslide using the monitored records of the Hyogoken-Nanbu earthquake by using DPRI-5, which has a shear box sized 180 mm in outer diameter, 120 mm in inner diameter, and 110 mm in height. The monitoring of earthquake nearest the Nikawa landslide was performed by JR (Japan Railways) Research Institute at the JR Takarazuka station. We estimated the seismic force acting on the sliding surface of the Nikawa landslide by the following procedures. Fukushima and Tanaka (1990) proposed an equation for the attenuation of peak ground acceleration that decreases with the distance from the active fault. According to Irikura (1996), the monitoring results of the Hyogoken-Nanbu earthquake also fitted the equation proposed by Fukushima and Tanaka. From the active fault map in urban area (Geographical Survey Institute, Japan, 1996), it is found that the JR Takarazuka station is 3 km and the Nikawa landslide is 0.5 km far from the active fault respectively. This means that the acceleration in Nikawa could be 1.47 times greater in Takarazuka. The Nikawa slope is a filled layer using the Osaka Group, and the monitoring site is on the stiff ground. Although the effect of softness is not investigated, it was pointed out that the average peak acceleration in soft soils is 140% of the average of all data (Fukushima & Tanaka 1990). So we used 2.0 (1.47x1.4) times of the monitored acceleration in Takarazuka for the Nikawa slope. Normal stress and shear stress components on the slope were estimated from three components of the monitored earthquake records in Takarazuka. And also it was assumed that the wave frequencies were kept the same as the

records, although it might be affected. Fig. 4 shows the synthesized seismic stresses together with the initial static stresses due to the self-weight of soil layer at the sliding surface for the simulation test. During the test, the sample was saturated by means of CO_2 and de-aired water with B_D = 0.95. After normally consolidated, a back-pressure of 58.8 kPa corresponding to the ground-water lever was applied. Thereafter, the sample was loaded by the seismic loadings shown in Fig. 4 in undrained condition.

Detailed information on the design of this apparatus as well as its operating principles can be obtained from Wang and Sassa (2002), and Sassa et al. (2003, 2004).

The test results are presented in Fig. 5. In Fig. 5a, the monitored normal stress is almost the same as the control signal. Fig. 5b shows the variation of excess pore water pressure. During the main shock (3 ~ 7 sec), the excess pore water pressure changed rapidly in response to the loading stresses. The bottom of excess pore water pressure indicates the excess pore water pressure built-up during the main shock. It should be noticed that excess pore water pressure kept increasing to a certain value even after the end of the main shock. Fig. 5c shows the variation of shear resistance and shear displacement. During the main shock, the sample failed because the loaded shear stress exceeded the shear strength of the soil. Shear displacement was still small during the main shock, however it increased rapidly after the main shock. The mobilized shear resistance gradually decreased, reasonably corresponding to the tendency of excess pore water pressure built-up after the main shock. Fig. 6 shows the stress path obtained in the simulation test. ESP means the effective stress path, while TSP means the total stress path. Because of possible delay of excess pore water pressure measurement during the period of high frequency, some stress points are distributed above the failure line. Although it is difficult to follow the process of each stress path with this figure, referring to the time series data, it is reasonable to describe the stress path as follows. At first, the stress path reached the peak strength failure line ($\phi_p = 39.6°$) and the soil failed. The state of shear zone then became residual. With progress of shearing after failure, the effective stress path turned towards the residual failure line ($\phi_r = 35.5°$). Shearing under a high effective stress could cause the grain crushing. This grain crushing process occurs within the shear zone, with resulting volume reduction under drained condition (as illustrated in Fig. 7), or with resulting pore pressure generation. Accompanying the generation of great excess pore water pressure, the effective stress path descended along the residual failure line to a very low effective stress level. The grain crushing continued until the effective stress became small enough in which the grain crushing could not take place any more. The apparent friction angle corresponding to the steady state after the sliding-surface liquefaction was 6.3 degrees. Therefore, an experimental explanation of this rapid landslide in the relatively gentle Nikawa slope (20 degrees) in dry season could be given by these test results.

Fig. 1 Locations of Nikawa and Tsukidate landslides

Fig. 2 Photos of the 1995 Nikawa landslide on Nishinomiya City (taken by Sassa)

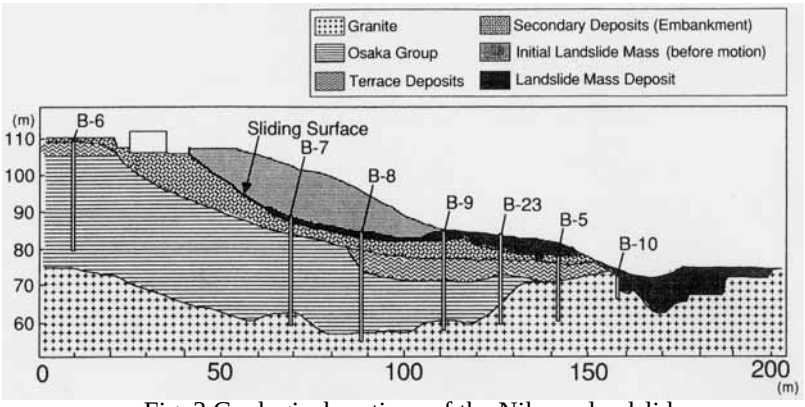

Fig. 3 Geological sections of the Nikawa landslide

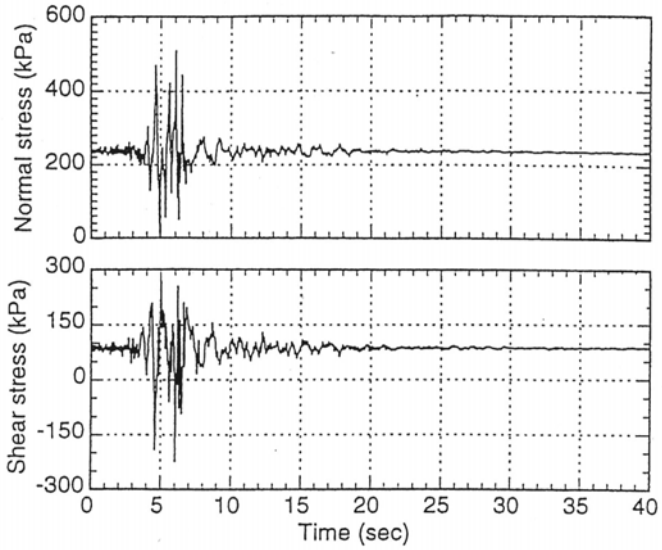

Fig. 4 Loading stress applied for the sample calculated from seismic record at JR Takarazuka station (by JR Research Institute)

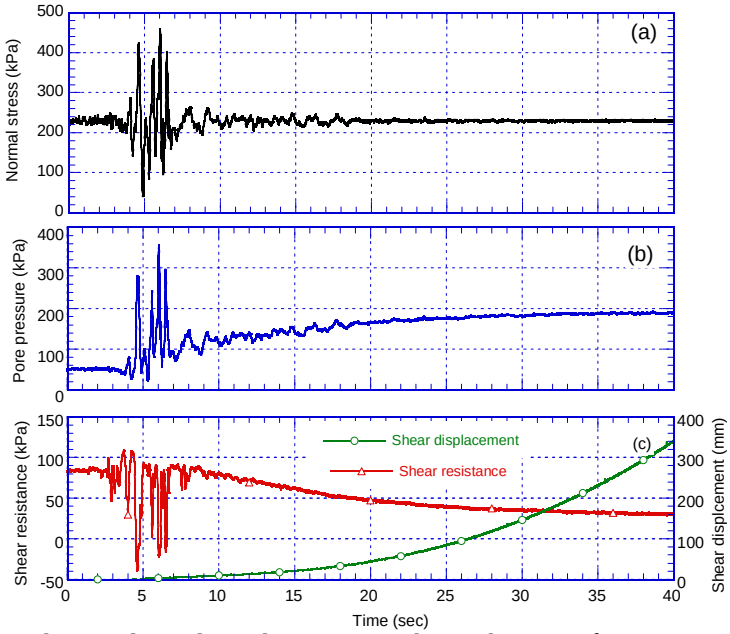

Fig. 5. Results of ring-shear undrained simulation test on the Osaka group formation in the Nikawa landslide (B_D = 0.99, D_r = 121.2%). (a) normal stress; (b) pore pressure; and (c) shear resistance and shear displacement.

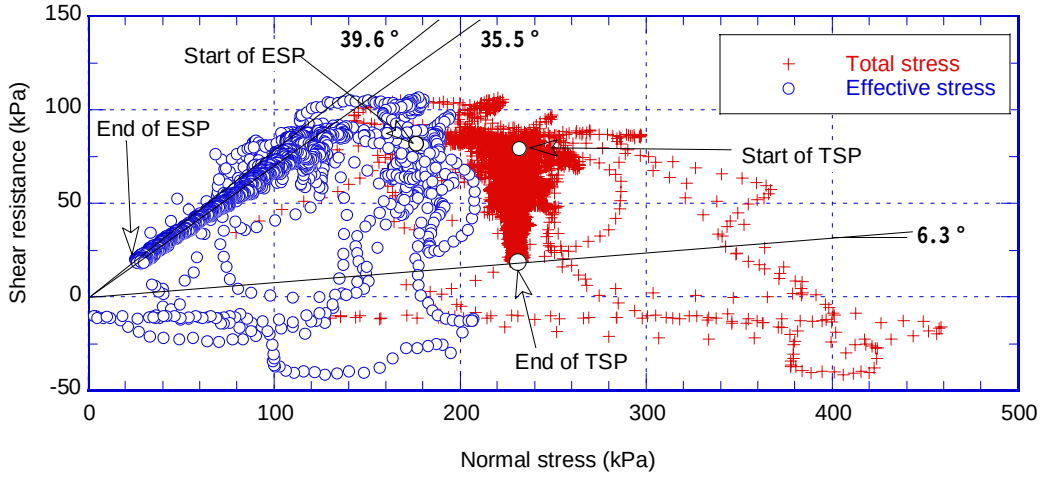

Fig. 6. Stress path for the ring-shear simulation test (ESP: Effective stress path, TSP: Total stress path)

To examine the grain crushing of this soil during shearing, the grain size distribution analysis was performed after 42 m shearing in the drained state. The samples were taken from the shear zone, from the upper part of the sample above the shear zone, from the lower part of the shear zone as well as the original sample. The results are plotted in Fig. 8. As indicated in this figure, the sample from the shear zone was the finest as the result of grain crushing.

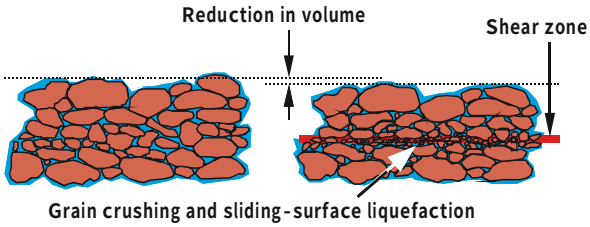

Fig. 7 Schematic illustration of the occurrence of sliding-surface liquefaction

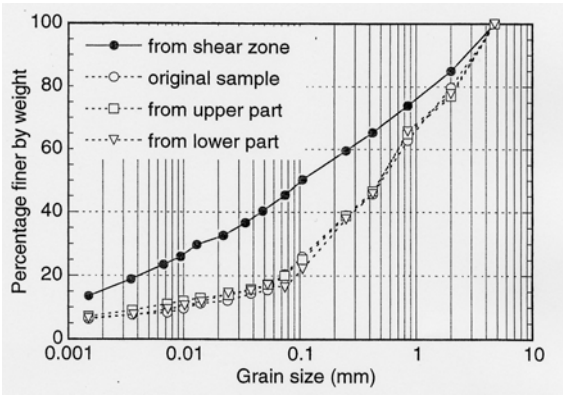

Fig. 8 Grain size distributions for the original sample, samples within, above, and below the shear zone, respectively, after sheared to 42 m under the normal stress of 196 kPa. Shear speed = 3 mm/sec.

2.2 Tsukidate Landslide triggered by the 2003 Sanriku-Minami Earthquake

During the May 26, 2003 Sanriku-Minami earthquake, a landslide was triggered on Tsukidate area, northwest of Sendai, the capital city of Miyagi Prefecture (See Fig. 1. thereinafter termed as Tsukidate landslide). Tsukidate landslide carried two houses away. Two people were partially buried by the displaced landslide mass. Fortunately, they were rescued by their neighbors. This landslide was triggered on a gentle slope of about 10 degrees. The displaced landslide mass traveled a long distance, and finally spread and deposited on a horizontal rice paddy, showing some typical characteristics of rapid long traveling flow phenomenon.

Fig. 9 shows an oblique side view (taken by Kokusai Kogyo Co. Ltd). From this photo, it is seen that the road on the right side is almost parallel to the landslide, indicating the nature of gentle slope. It is also noticed that almost all of the displaced landslide mass slide out of the source area and deposited on a horizontal rice paddy. Fig. 10 is the view from the toe of the landslide, which was taken four days after the event (at our survey time). The source area was covered by blue sheet for the prevention of possible second disaster during rainfall. The bamboos on the source area originally were transported with the landslide mass; however, most of them were standing almost vertically on the rice paddy with very thin landslide mass below them.

From these figures presented above, a question may be raised why this landslide could be triggered on such a gently slope and travelled such a long distance. To examine the triggering mechanism, it is necessary to have a better understanding on the geological background of the slope. Comparing the present contour map of this area to that of about 40 years ago, it is made clear that the source area of this landslide might be located on the fillings, where a

gully was buried for cultivation. This could be seen from Fig. 11, where the contour maps obtained in 1962 and 2001, respectively, were presented. Within the cycle in Fig. 11a where Tsukidate landslide was triggered, a gully could be identified easily. However, this gully was buried about 40 years ago, and there was no such gully in the same area (see Fig. 11b).

Portable dynamic cone penetration (PDCP) tests were performed along the centre line of the landslide to examine the strength properties of the soils on the source, travelling path as well as the deposition areas (Fukuoka et al. 2004). Fig. 12a presents the plan of the landslide where the locations of PDCP test points are superimposed. Among these test points, three tests, No. 6, No. 7, and No. 9 were located out of the landslides; No. 6 and No. 7 were located on the upper part of the scarp, while test No. 9 was 44 m east of the scarp. The test results for these three locations are presented in Fig. 12b in the form of soil depth against the deduced *N* value. Usually, greater deduced *N* value means greater shear resistance, which depends on the soil type, soil density, etc. It is inferred that the penetration for test No. 6 had been performed within the fillings, where the deduced *N* values were very small on the whole penetrating process of 400 cm. Test No. 7 showed a sharp increase in the deduced *N* value after the penetration depth of about 330 cm, indicating that the penetration had reached the bedrock. Test No. 9 showed a sharp increase in *N* value with increase of soil depth within the soil depth of 100 cm. From these tests results, it could be inferred that the source area of this landslide was located within the fillings, and these fillings had low shear resistance.

Using a total station, a central longitudinal section of the landslide from the source area to the deposited area of the paddy was surveyed (Fig. 13). The landslide descended 27 m over a horizontal distance of 180 m (from the source area to the toe of the landslide on the paddy). The original ground surface marked in thin line was inferred according to the shape of the neighbouring ground surface. From Fig. 13, it is seen that this landslide originated from a gentle slope with an inclination of about 10 degrees. The apparent friction angle, which is the slope angle of the line (marked in broken line) from the head scarp to the toe of landslide, was approximately 7.3 degrees.

To examine the triggering mechanism of the landslide, samples were taken from the source area from the fillings, which was mainly composed of pyroclastic deposits. Fig. 14 presents the sampling site on the left side (see from the upper slope to down slope) of the landslide. As revealed by this photograph, the pyroclastic deposits changed its colour from brown (due to oxidization) to blue-grey (due to deoxidisation). This means that the iron contained in the soil was not oxidized due to the long term existence of ground water. Therefore, it was concluded that abundant ground water existed within the source area. Because it is apparent that liquefaction phenomenon was the main reason for this long runout landslide, laboratory tests were performed on these samples from the source area with emphasis on the liquefaction potential of the filling soils.

Undrained cyclic ring-shear tests had been performed on the samples from the source area. During the sample preparation, gravels in the sample greater than 2 cm were sieved out. The grain size distribution of the sample after sieving is presented in Fig. 15. The sample in the field had the specific gravity of 2.61, dry density of 1.1 g/cm^3, void ratio of 1.38, and a unit weight (γ_t) of approximate 15.7 kN/m^3 with a water content (at the sampling time) of 45.7% by weight. During tests, the sample was saturated and normally consolidated under the stress state corresponding that at the sliding surface on the source area shown in Fig. 13.

Because the tests aim to examine the liquefaction potential of the soil on the source area, here a thickness of 3 m was used for the displaced soil mass in the source area. In calculating the normal stress and shear stress acting on the sliding surface, a slope angle is measured as 13.5 degrees approximately from Fig. 13, and a saturated unit weight (γ_{sat}) for the soil mass in the field was calculated as 16.5 kN/m^3 by the measured properties of sample. After consolidation, a seismic shear loading with great amplitude of shear stress (considering that this landslide area was very close to the earthquake epicenter) was applied to the sample under undrained condition, while the normal stress was kept constant.

The test results are presented in Fig. 16, in the form of time series data (Fig. 16a) and effective stress path (Fig. 16b). As shown in Fig. 16a, the shear strength showed a great reduction within one cycle of cyclic loading, and reached a small value of approximate 9 kPa, while the monitored pore-water pressure kept increase with time and finally reached almost the same as the normal stress. Shear displacement reached about 49 m within the shear time of 115 seconds. From Fig. 16b, it is seen that the effective stress path reached the failure line in the first cycle of shearing, and thereafter shifted leftwards almost horizontally. This probably was due to the fact that the shear failure was localized on the shear zone, and the pore-water pressure generated within the shear zone was not monitored correctly (detailed information on the pore pressure measurement system could be obtained in Sassa et al. 2004). It is also noticed that most of the pore-water pressure was built up after the shear failure, i.e, with progress of shearing, indicating the sliding surface liquefaction phenomenon. The apparent friction angle was about 7.5 degrees, showing a good consistency with the apparent friction angle of the landslide in Fig. 13.

Fig. 9 Oblique side view of the landslide (Photo courtesy of Kokusai Kogyo Co., Ltd).

Fig. 10 View from the toe of Tsukidate landslide.

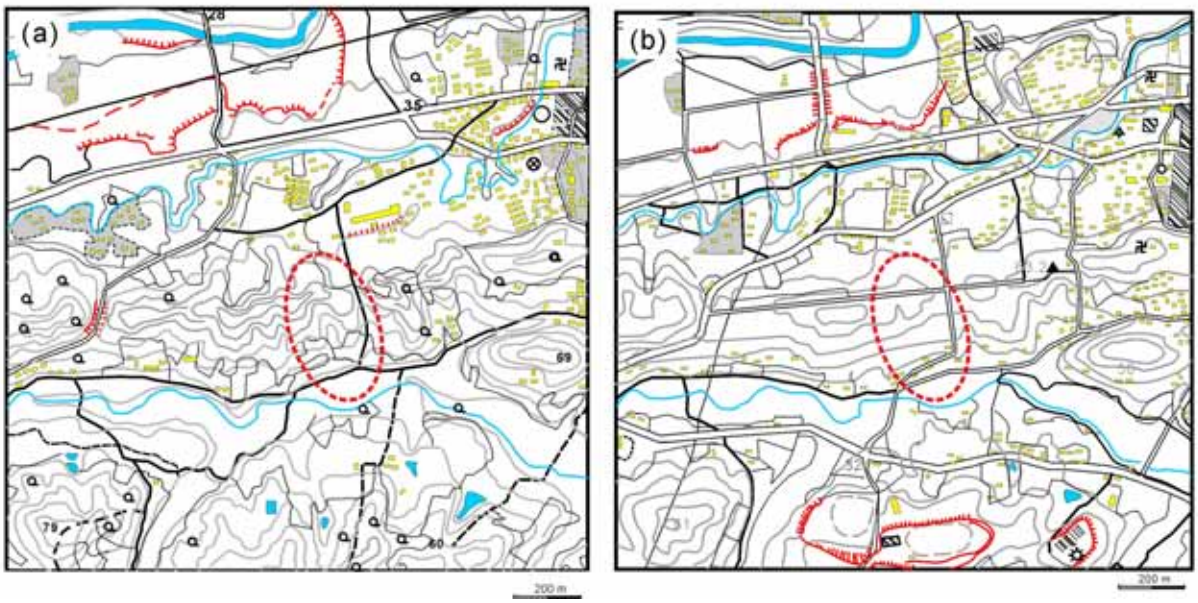

Fig. 11 Counter maps of Tsukidate area in 1962 (a) and 2001 (b), respectively. Tsukidate landslide was triggered within the cycle on May 2003.

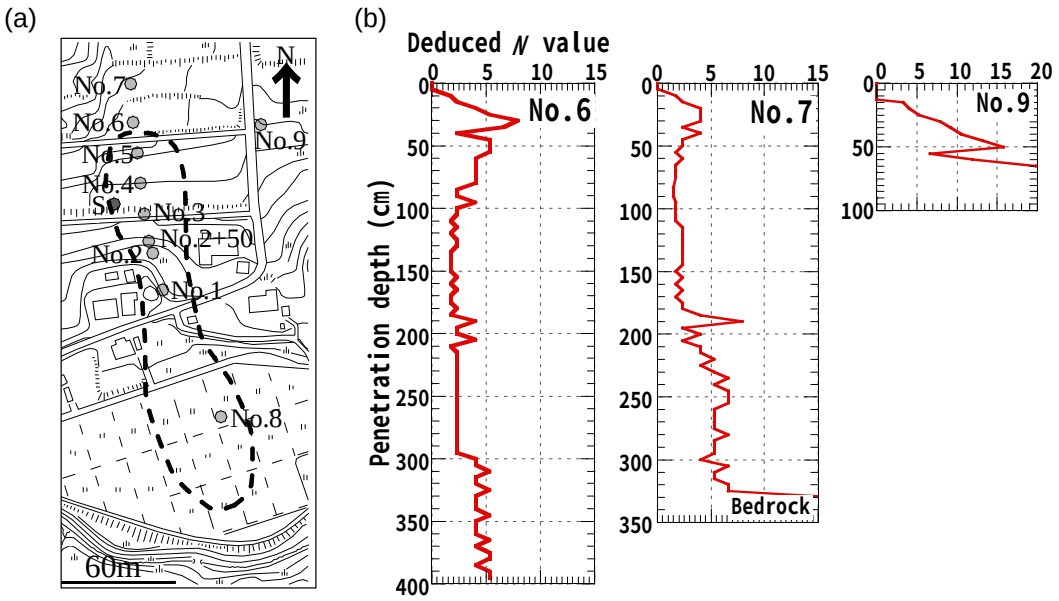

Fig. 12 (a) Contour map of Tsukidate landslide area after the earthquake obtained by airborne laser scanner (Courtesy of Aero Asahi Corporation, Japan. Contour interval is 50 cm, and the red line shows the landslide area), and the locations of Portable dynamic cone penetration tests; (b) In-situ penetration test results: deduced *N* value against soil depth.

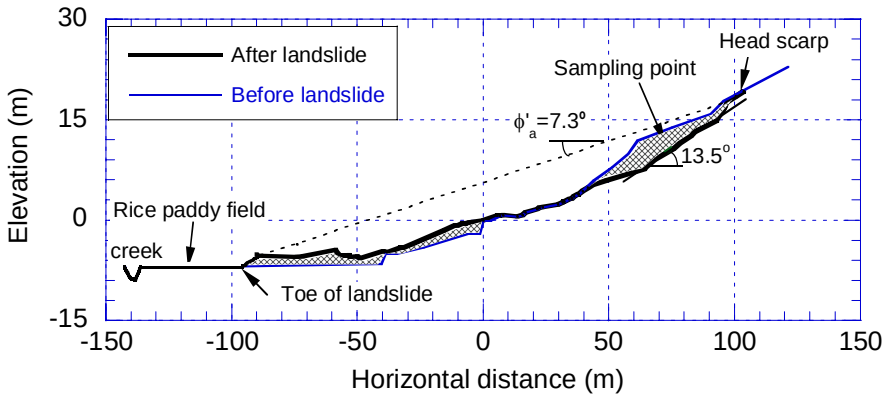

Fig. 13 Longitudinal cross section of Tsukidate landslide.

Fig. 14 Sampling on the source area

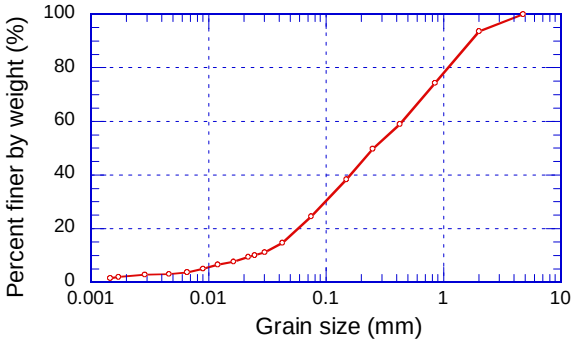

Fig. 15 Grain-size distributions of sample from the source area.

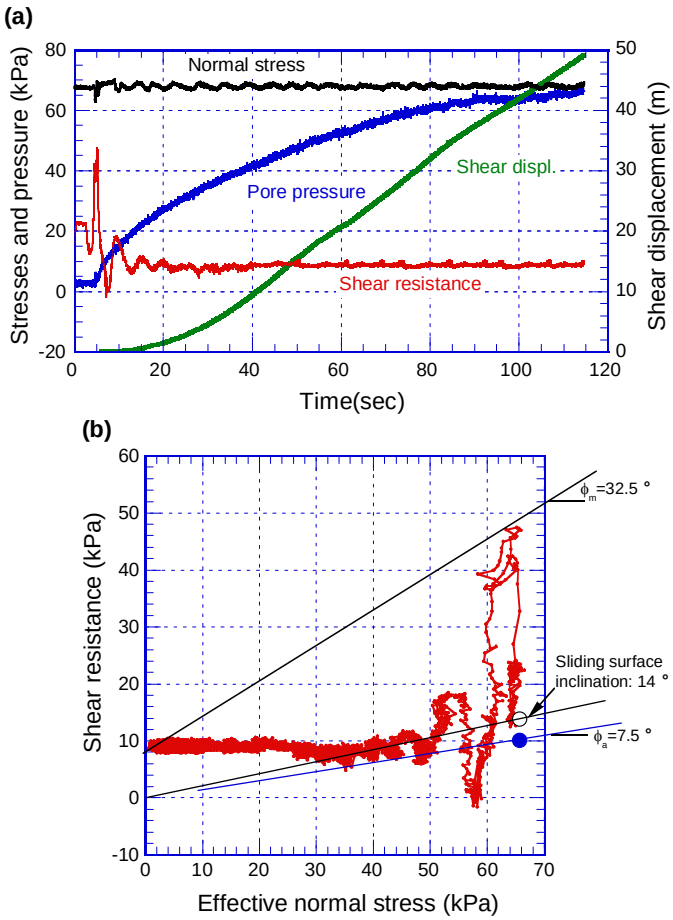

Fig. 16 Undrained cyclic ring shear test on the saturated sample taken from the source area (B_D = 0.97). (a) time series data of normal stress, shear resistance, pore-water pressure, and shear displacement; (b) effective stress path.

3. Minamata Landslide triggered by the 2003 Heavy rainfall, Kumamoto Prefecture

On 20 July 2003, a landslide occurred in an andesitic weathered lava layer on a mountain slope of 31-32 degrees in Minamata City, Kumamoto Prefecture, Kyushu Island, Japan. It was triggered by a heavy rainstorm with 314 mm total rainfall and a maximum rate of rainfall of 91 mm/hour. The slide mass entered a torrent, where it was transformed into a debris flow that struck a village along the torrent, destroying 15 houses, killing 15 people, and injuring an additional six people. Fig. 17 presents a view of the debris flow. The initial slide can be seen at the head of the debris flow. Apparently, this debris flow was triggered by the slide, and the landslide mass flowed downstream along the torrent, increasing its volume by entraining material from the channel and weathered surface soils of the mountain slopes on both sides of the channel. Fig. 18 shows the central

section through the initial slide surveyed by a non-mirror total station. Based on a topographic survey made after the landslide occurred, the initial slide was estimated to have occurred along a failure surface with an inclination of 26.5 degrees and depth of approximately 10-12 m.

Two samples were collected, one from the weathered andesitic lava, one from tuff breccia. The andesitic lava sample was taken under the sliding surface near the head scarp at the mark of Sample A in Fig. 18. The tuff breccia sample was collected from the mountain slope near the channel in the flank of the initial landslide at the mark of Sample B (projected to the central cross-section) in Fig. 18.

Fig. 17 Aerial oblique view of the 2003 Minamata debris flow

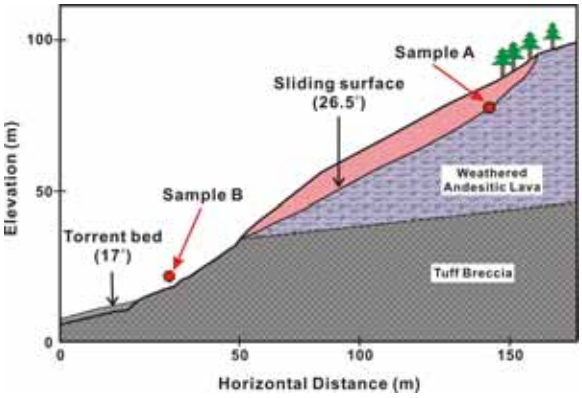

Fig. 18 Central section through the Minamata landslide in its original state

This initial landslide occurrence was geotechnically simulated using the DPRI-5 ring shear apparatus. The initial stresses on the sliding surface were reproduced in the apparatus; then, the pore pressure was gradually increased simulating the rise of ground-water level during rainfall. In natural slopes, the ground-water rise would not be rapid; thus, the undrained loading condition was not used. To simulate drained ground-water conditions, water pressure supplied to the shear box through the upper drainage valve was gradually increased. Thus, water pressure was controlled, but the water was free to move through the upper valve. Therefore, the sample was subjected to a natural drained condition. If pore pressure was generated in the shear zone during loading, it drained naturally through the upper valve. The test result is shown in Fig. 19. After the stress path reached the failure line, it suddenly dropped to a much lower value. Thereafter, the shear resistance slightly recovered to a certain value.

This action of rapid drop of shear resistance was interpreted as follows: when shear failure occurred, volume reduction took place due to grain crushing and the resulting failure of the soil structure; this caused rapid excess pore-pressure generation. However, excess pore pressure was not monitored by the pore-pressure transducer because the upper valve was open and the transducer was not located at the shear zone. Therefore, the stress path deviated from the failure line and dropped vertically.

The high pore pressure in the shear zone dissipated through the upper valve, but some excess pore pressure remained as the combined effect of pore-pressure generation within the shear zone and pore-pressure dissipation from the shear zone. The pore pressure generation speed was likely to have decreased from the immediate post-failure condition, while at the same time, the pore pressure dissipation speed was maintained. Therefore, the shear resistance recovered somewhat and settled to a certain value. The result gave an apparent friction angle of 9.7 degrees.

This test is called a naturally drained test because generated excess pore pressure is naturally drained from the shear zone to the upper valve. After the naturally drained test, the sample was again consolidated by dissipating the generated pore pressure. Then, slow shearing was applied. After reaching the failure line, the normal stress was decreased very slowly to maintain the drained condition, continuing slow movement without generating any pore-water pressure. This test determined the status of the failure line during motion, as shown in Fig. 19. This test gave 32.9 degrees as the friction angle during motion.

These test results show that the andesitic lava deposit was subjected to high excess pore-pressure generation due to post-failure shearing and a low apparent friction angle of 9.7 degrees was mobilized. This means that the Minamata slide rapidly reached the torrent bed. The gradient of the torrent bed at the toe of the slope was 17 degrees; so, the landslide

necessarily continued to move downstream and changed into a debris flow.

Loading by the failed slide mass onto the pre-existing torrent deposits was first modelled by Sassa et al. (1997) as shown in Fig. 20. The slide mass moved down the slope (I), and applied load onto the torrent deposits at the foot of the slope (II). Because a surface water stream or subsurface flow existed and some of the deposits were saturated, the torrent deposit was sheared by undrained loading and transported downstream together with the sliding mass (III). Let us consider a column of unit width, which is a part of the torrent deposit. In the position (I) of the sliding mass, the weight of the column (W_0) was in effect. When the sliding mass rode on to the torrent deposit (II) with a certain velocity, it provided dynamic loading of the column. Here, we assume that the applied stress on the torrent deposits was as the sum of the static stress, ΔW, (load due to the weight of the sliding mass) and the dynamic (impact) stress, F_d, working in the direction of motion of the sliding mass.

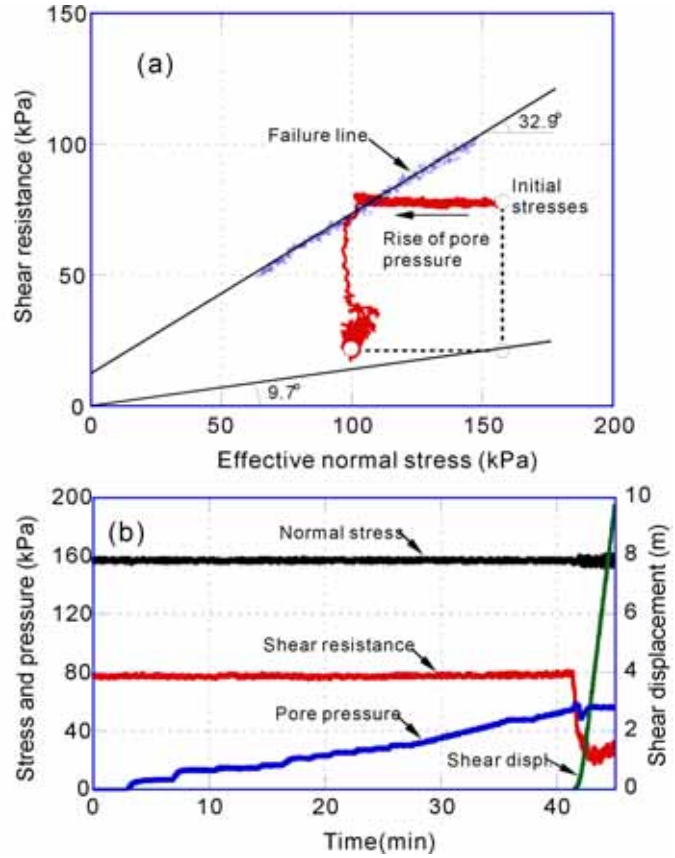

Fig. 19 Results of tests to simulate the initiation of the Minamata landslide ($B_D = 0.86$)

The stress working on the bottom of the soil column is presented in Fig. 20(b). The initial stress is expressed by the point "A", which corresponds to the position (I) of the sliding mass in Fig. 20(a). If no excess pore pressure is generated during loading, the stress point moves to point (C) by adding the static stress (ΔW) to the initial stress. In addition, by adding the dynamic stress (F_d) to the static stress, the total stress moves to point (B). Therefore, the stress path in the actual field case tends to move from point A to point B. However, when the stress path reaches the failure line, it moves along the failure line (Fig. 20b), because the stress path cannot exceed the failure line. At the point at which the dynamic stress reduces to zero, the total stress moves back to the stress point (C), namely the sum of W_0 and ΔW. Denoting the angle of thrust at collision with the torrent deposit as α and the dynamic stress as F_d, using a dynamic coefficient $\boldsymbol{k_d}$ = ($F_d/\Delta W$), the dynamic shear stress and normal stress are expressed as:

$$F_d \cos\alpha = \tau_d, \qquad F_d \sin\alpha = \sigma_d \qquad (1)$$

The stress path from A to B to C is the total-stress path in the case where no pore-pressure is generated. However, excess pore pressure is likely to be generated during loading and also during shearing after failure. In this case, the effective-stress path will deviate from the total-stress path as a curved line from A to D.

When the landslide mass moves from the steep

slope to a gentle slope, the angle α in Fig. 20 is great, but when the landslide mass (i.e., the debris flow) travels along the torrent (as shown in Fig. 21), the angle α is zero. Another test was conducted to simulate the landslide (debris) masses as it moved onto the torrent deposits and/or the surface soil layer of both slopes assuming the depth of moving mass was about 10 m, the gradient of the torrent bed was 15 degrees, the depth of the torrent deposit or surface soils was 2-4 m, and the dynamic coefficient was 0.9. Because of such rapid loading by the fast-moving slide mass (more than 10 m/sec), the test was carried out under undrained conditions. The sliding surface was formed inside the torrent deposits which were composed of andesitic lava or tuff breccia. The surface soil layers of mountain slopes near the upper and middle part of torrent was mainly tuff breccia, though the lower part of the torrent was composed of non-volcanic sedimentary rocks. Therefore, two undrained loading tests were conducted for deposits of tuff breccia and those of andesitic lava.

The test result of Fig. 22 shows the case for tuff breccia, in which the torrent deposit and/or the surface soils were sheared and moved together with the original slide mass. Only 18.5 kPa was necessary as additional shear stress to cause shear failure and the mobilized apparent friction angle was only 1.9 degrees in this rapid and undrained loading condition as estimated from Fig. 22(b). The test result of Fig. 23 shows the case for andesitic lava. This is stronger, the additional necessary shear stress was 45.5kPa and the mobilized apparent friction angle at the steady state was 3.4 degrees. Both cases suggested that such saturated deposits were scraped and included in the moving mass. However, if the material were not fully saturated, it probably would not be scraped as the case study in the Kameyama landslide, Hiroshima, Japan (Wang et al. 2003)

To examine and interpret the actual phenomena, additional investigation and testing are necessary. However, this test has shown that this apparatus and its application provide an effective tool to study the mechanism of slide-triggered debris flows and the increase of landside mass by material entrainment during the flow.

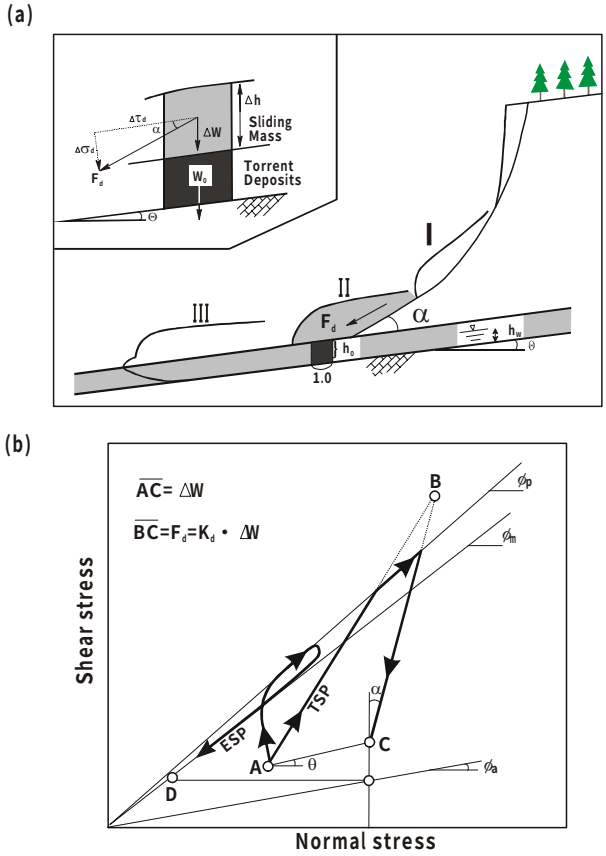

Fig. 20 Model of the landslide triggered debris flow (Sassa et al 1997). (a) Illustration of the model; (b) Stress path of the torrent deposit during loading. α: angle of thrust between the slope and the torrent bed; F_d: dynamic stress; k_d: dynamic coefficient (F_d / ΔW).

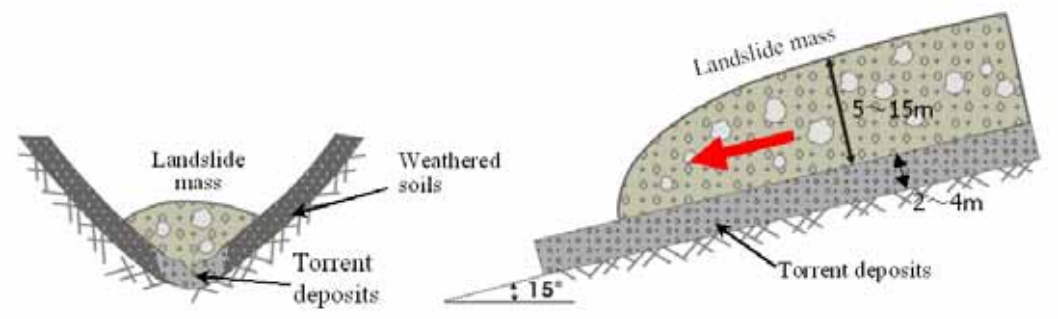

Fig. 21 Illustration of moving landslide mass along a torrent

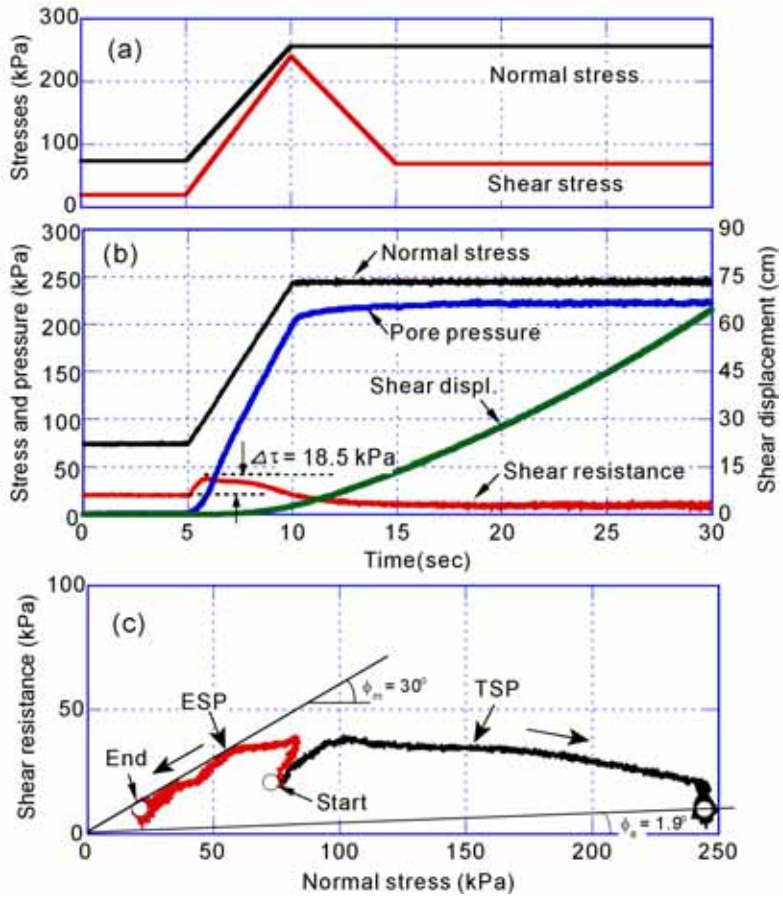

Fig. 22 Results of a test to simulate undrained loading of the tuff breccia deposits in the Minamata landslide (B_D=0.89)

4. Mechanisms of urban landslide disasters and risk identification

As revealed by the above-mentioned case studies, these urban landslide disasters triggered by earthquakes were due to the sliding surface liquefaction. Usual liquefaction (mass liquefaction) (Sassa, 2000) occurs on very loose deposits with full saturation. So the soil layer on slopes susceptible to mass liquefaction are limited. While the sliding surface liquefaction could occur in loose, medium or even dense sandy materials so long as grain crushing in the shear zone will result in volume shrink. Then, the risk of sliding surface liquefaction exists in a wide area. The examples introduced are granitic debris (fill), andesitic debris, and pyroclastic deposits. The sliding surface liquefaction needs a saturated layer, while saturated layers are usually formed in

gentle slopes. All these cases here had gentle sliding surfaces at least in the lower half of initial landslide mass. All these disasters were partly related to regional development. Houses were constructed on/near the layer susceptible to the sliding surface liquefaction. Therefore, for risk identification of catastrophic landslide disasters due to the sliding surface liquefaction for concerned locations in planning, the following three aspects should be considered.

1) Are materials in slopes concerned susceptible to the sliding surface liquefaction?

2) Are slopes concerned steeper than the mobilized apparent friction angle in the steady state?

3) Are there houses or other objectives constructed in the landslide moving area estimated from the apparent friction angle?

The apparent friction angle of a soil at steady state in undrained condition could be obtained through ring shear tests. The mobilized apparent friction angle as the average value including both of source area and moving area in Nikawa and Tsukidate were less than 10 degrees. This number can be a rough index of dangerous area for simple consideration. However, the value will be much changed according to type of soils, saturation degree and depth of sliding mass.

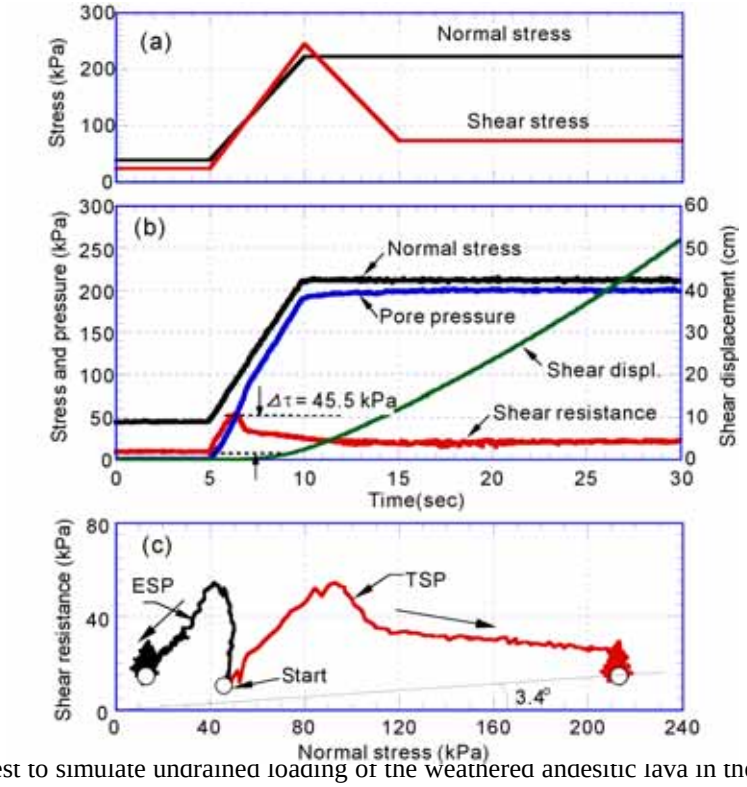

Fig. 23 Results of a test to simulate undrained loading of the weathered andesitic lava in the Minamata landslide (B_D = 0.97)

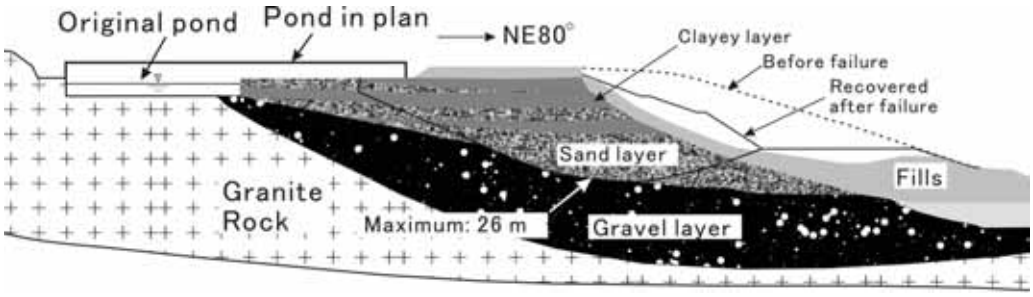

Fig. 24 Cross section of Nikawa slope

5. Landslide Risk Assessment of Urban Areas

5. 1 Nikawa Slope Case

As a project of the International Programme on Landslides (IPL) coordinated by the International Consortium on Landslides (ICL), M101: Areal Prediction of earthquake and rain induced rapid and long-traveling flow phenomena (APERITIF) was

proposed and approved as an on-going member project by the first Session of Board of Representatives of the ICL. As a part of APERITIF project, we investigated to assess the catastrophic landslide risk in the slope area above the Nikawa landslide assuming that another earthquake will attack this area in the same scale as the Kobe earthquake.

5.1.1 Properties of the Nikawa Slope

Fig. 24 presents a cross section of the central part of Nikawa slope along the direction of NE80°. The boring investigation revealed that the base rock of the slope is granite; above the base rock is granitic gravel layer (weathered granite). Overlaid on the granitic gravel layer are the granitic sandy layers (there are some clayey layers within them) and fillings. Note that the matrix of gravel layer is mainly composed of fine sand and silt with very lower permeability. The overall permeability of gravel layer is about 10^{-5} cm/sec, through the inner boring measuring method, while that for the sandy layer laying above the gravel layer is 10^{-4} cm/sec. When earthquake comes, a potential sliding surface is inferred to pass through the interface between the sandy layer and gravel layer, as shown in Fig. 24, where the maximum depth is 26 m, and the average angle of the potential sliding surface is about 20 degrees. Ground water is 16 m above the potential sliding surface at the point of 26-m soil depth. Considering that shear failure could occur in both layers, tests were then performed on the samples from the boring core for these two layers, respectively. Hereinafter, we call the samples from the granitic gravel layer as GL, and those from the sandy layer as SL in this report. Fig. 25 shows the grain size distribution of the samples.

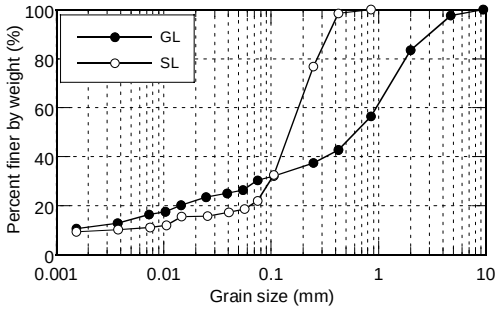

Fig. 25 Grain-size distributions of samples from the sandy layer (SL) and gravel layer (GL), respectively

5.1.2 Test Condition & Test Procedures

The main question is whether or not this slope can suffer sliding surface liquefaction failure when a supposed earthquake as great as the 1995 Hyogoken-Nanbu earthquake comes. Hence, the same seismic waves as that used for the simulation test for Nikawa landslide were used. An ideal infinite slope of 20 degrees was assumed as in Fig. 26 with a soil depth of 26 m and ground water table 16 m above the potential sliding surface. And then the possible seismic loadings acting on the sliding surface during earthquake were synthesized using the same method for the simulation test on Nikawa landslide. Therefore, a maximum acceleration of 1250 gal was inferred acting on the slope in Fig. 26. In the computation, unit weights of 20.6 kN/m^3 and 17.6 kN/m^3 were used for the soil layers below and above the ground water table, respectively. Fig. 27 presents the synthesized seismic loadings on the potential sliding surface.

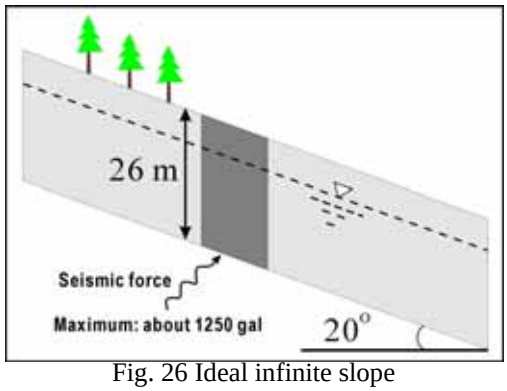

Fig. 26 Ideal infinite slope

Ring-shear apparatus, DPRI-5, was also used for this research. During tests, the samples were saturated with $B_D \geq 0.95$. After normally consolidated, a back-pressure of 154 kPa corresponding to the ground-water level was applied. Thereafter, the sample was loaded by the seismic loadings shown in Fig. 27 in natural drained or undrained conditions. Note that natural drained condition refers to the situation that the upper drainage tube of the shear box is open to permit the dissipation of pore-water pressure during shearing in this paper.

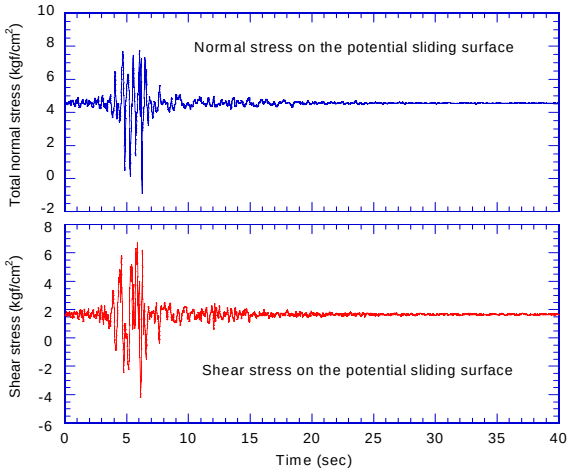

Fig. 27 Synthesized seismic loadings on the inferred potential sliding surface

5.1.3 Test Results and Discussions

Undrained shear tests on saturated samples

Undrained shear tests were first performed on the saturated SL and GL, respectively. Test results showed that sliding surface liquefaction phenomena could be triggered in both samples with high pore-water pressure generation and accelerating motion. To have a brief understand of the undrained response of these samples to the applied seismic loadings, here the results of one test on SL are presented in Fig. 28, where the time series data of normal stress, shear stress, pore pressure, as well as shear displacement are plotted in Figs. 28a and 28b. Fig. 28c shows the effective stress path (ESP) and total stress path (TSP). It is seen from Fig. 28a, the monitored normal stress is almost the same as the control signal in Fig. 27. The monitored value for shear strength shows the applied shear stress before failure, but after failure, it presents the mobilized shear resistance, because the target value for modified shear stress could not apply to the sample completely. Hence, the shear strength in Fig. 28a behaved differently from the control signal in Fig. 27. During the main shock, the shear strength showed a certain of reduction, the pore water pressure increased rapidly. Shear failure was resulted, and shear displacement increased consequently. Even after the seismic loadings ceased, shear displacement accelerated to increase, while pore pressure elevated slowly, and finally tended to a constant.

From the ESP in Fig. 28c, it is noticed that the initial effective stress state was very close to the failure line. This means that a small increase in pore-water pressure (about 59 kPa, if normal stress and shear stress are kept steady) or in shear stress (about 39 kPa when normal stress and pore pressure are kept steady) could lead to the shear failure of the sample. This was facilitated by an increment in pore water pressure more than 150 kPa during the main shock (see Fig. 28b). After failure, the shear strength reduced along the failure line towards zero with progress of shear displacement. Although there are some points of ESP laid above the failure line, probably due to the possible delay of pore water pressure measurement during high frequency period, this ESP showed a typical path for sliding surface liquefaction failure phenomenon (Sassa 1996) Meanwhile, we can see that the TSP never crossed the failure line even in the seismic loading period, indicating that if there is neither initial pore water pressure nor excess pore-water pressure generation, the sample can not suffer shear failure.

Although the test on saturated gravel layer showed similar phenomena, the time series data revealed that the main part of excess pore-water pressure was generated after failure with progress of shear displacement (see Fig. 29), while lesser was built up during the main shock (about 74 kPa).

Naturally Drained Shear Test Results

In the analysis of liquefaction triggered by earthquake, rainfall, or some other factors, it is deemed that the loadings are applied in such a short time that the generated pore water pressure could not dissipate immediately, such that almost all the laboratory works, with a few exception, have been trying to mimic the soil behaviour under undrained conditions. In fact, soils in a natural slope cannot be truly undrained, especially in the post-failure process of sliding, where the pore water pressure is generated with progress of shear displacement and dissipated until progress of time. In this sense, naturally drained shear tests may be more close to the practical situation. Therefore, naturally drained seismic loading tests also were conducted on these two samples mentioned above. During test, the samples were first saturated (B_D = 0.98 and 0.95 for GL and SL, respectively). After consolidation and application of backpressure, the samples were loaded by the seismic loadings, keeping the drainage tube in the top of the shear box open, while the drained tube in the bottom of the shear box closed.

The results of naturally drained test on SL are presented in Fig. 30, where the time series data of normal stress and shear stress are shown in Fig. 30a, those of pore water pressure and shear displacement in Fig. 30b. As indicated in Fig. 30b, the pore-water pressure increased a little after the main shock, and even showed a transient increase after the main shock. However, it dissipated soon with time. Shear failure was initiated during the main shock. Nevertheless, the shear motion ceased after a certain of displacement (approximately 67 mm), and the mobilized shear strength after the main shock showed almost no reduction, i.e., no liquefaction failure was initiated (Fig. 30a). This means that for SL, although pore-water pressure was generated within the shear zone, pore pressure dissipation speed was greater than pore pressure generation after main shock. Therefore, the pore pressure in the shear zone gradually dissipated and stopped the shear displacement.

The test results for GL showed quite different phenomena (Fig. 31). After the main shock, the shear displacement increased continuously, showed an accelerating failure process (see Fig. 31b). The shear strength reduced gradually with time (Fig. 31a), showed typical sliding surface liquefaction failure. The great reduction in the shear resistance could be attributed to the great generation of pore water pressure within the shear zone. However, in Fig. 31b it is noticed that the monitored pore pressure was not so high in the acceleration of shear displacement. This could be interpreted as follows: during this period, because the drainage tube is open, and also the shearing was localized in the shear zone while the pore pressure was measured through a gutter located 2 mm above the shear surface (detailed pore pressure

measurement system can obtained from Sassa et al. 2003), the monitored pore water pressure was not credible enough. It is inferred that high pore water pressure was built up within the shear zone as the combination result of the generation and dissipation. The dissipation of generated pore water pressure from the shear zone could be much lower than that of the sandy layer, due to the lower permeability. Therefore, in the case of GL, pore pressure generation speed was greater than the pore pressure dissipation speed even after the main shock. Thus, pore pressure should have been built up during the progress of shear displacement.

Although the naturally drained simulation tests presented in Figs. 30 and 31, were differing from real slope condition, where the thickness of the soil above the shear zone might be quite greater than that in the ring-shear box (about 5 cm above the shear zone), from Figs. 30 and 31, it can be concluded that GL is easier to suffer liquefaction failure with long travelling distance in natural slope state.

From these above-introduced test results, following conclusions could be drawn:

(I) If the soil layer could slip under the excess pore-water pressure built up immediately after the main shock of earthquake, generation of excess pore-water pressure could be continued after the main shock due to the grain crushing with progress of shearing. In case the pore pressure generation speed is greater than the pore pressure dissipation speed in the progress of post-main shocking shearing, the sliding surface liquefaction phenomenon could be resulted in;

(II) If the soil layer could not slip even under the excess pore-water pressure built up immediately after the main shock of earthquake, sliding surface liquefaction phenomenon could not be triggered;

(III) To prevent the triggering of sliding surface liquefaction, it is possible to lower the initial ground water table such that the slip could not be triggered, even though a certain of excess pore-water pressure could be built-up during earthquake.

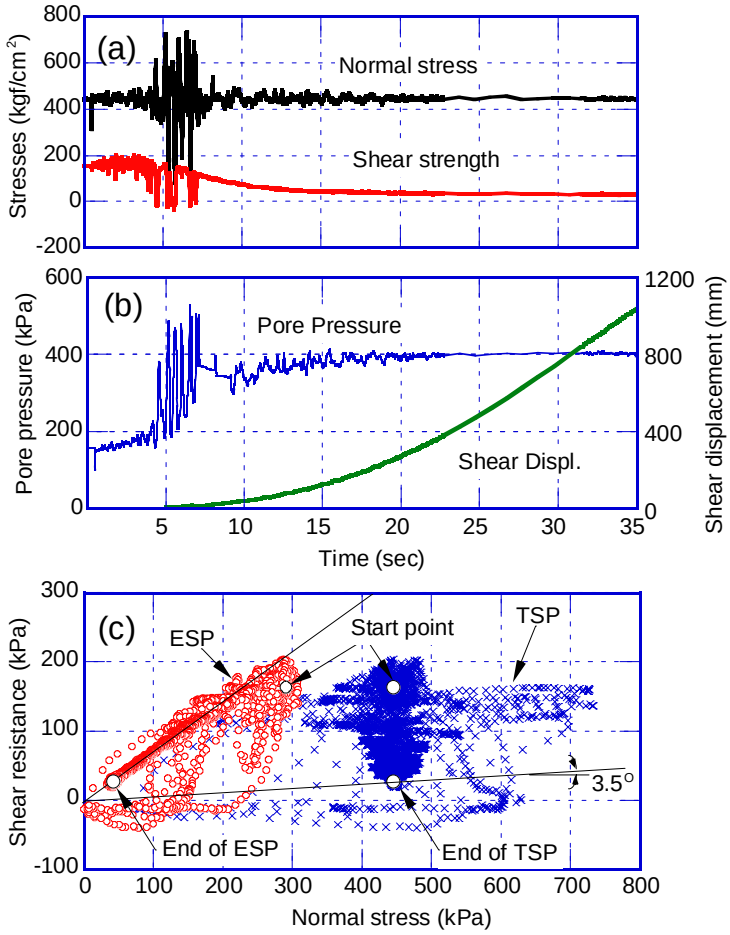

Fig. 28 Undrained cyclic tests on saturated sandy layer (B_D = 0.99, initial dry density: 15.2 kN/m^3). (a) Time series data for normal stress and shear stress, (b) Time series data for pore water pressure and shear displacement, and (c) Stress path

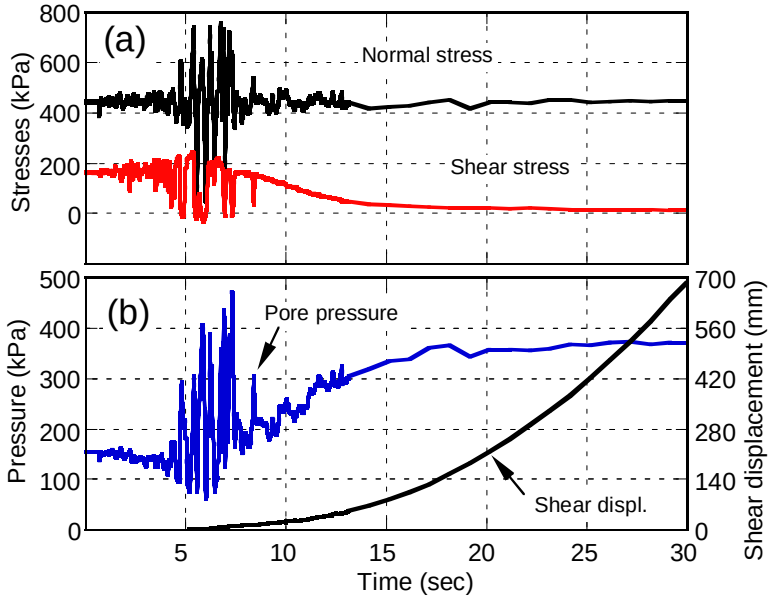

Fig. 29 Time series data of shear stress, pore water pressure and shear displacement for the undrained cyclic tests on saturated gravel layer (B_D = 0.98, initial dry density: 17.4 kN/m^3)

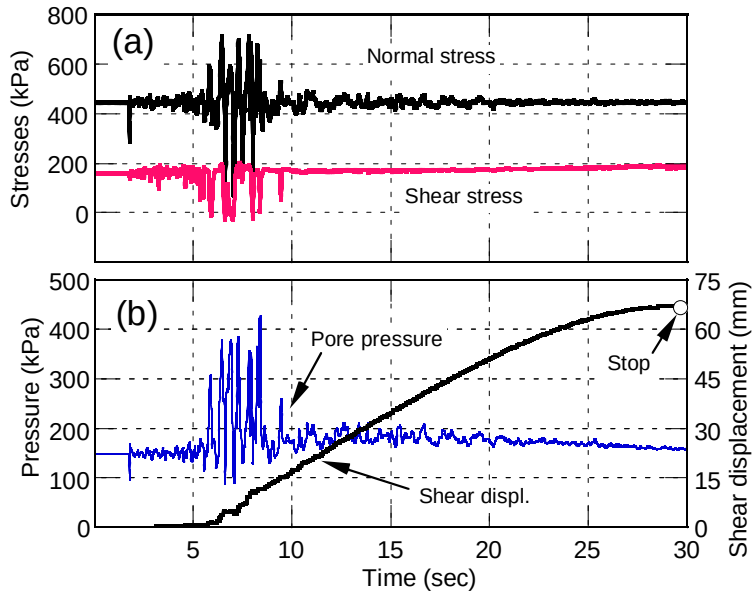

Fig. 30 Time series data for naturally drained cyclic test on saturated sandy layer (B_D = 0.95)

Basing on the consideration of III, a method (as shown in Fig. 32) was proposed to prevent the occurrence of sliding surface liquefaction phenomenon on the Nikawa slope area. A trench with great depth of around 10 m was planed on the upper part of the slope, through which the ground water from the mountain side and lateral sides could be drained out so to lower the ground water table, also downward drillings could be dug so to prevent the elevating of pore-water pressure within the rock cracks in the granite rock during earthquake. Through this method, it is expected that ground water table could be lowered 5 m in average. This lowered value is greater than the excess pore-water pressure built up during the main shock, and then the slope could keep the safety factor as the same or greater than the present one, even under the increased pore pressure during the main shock.

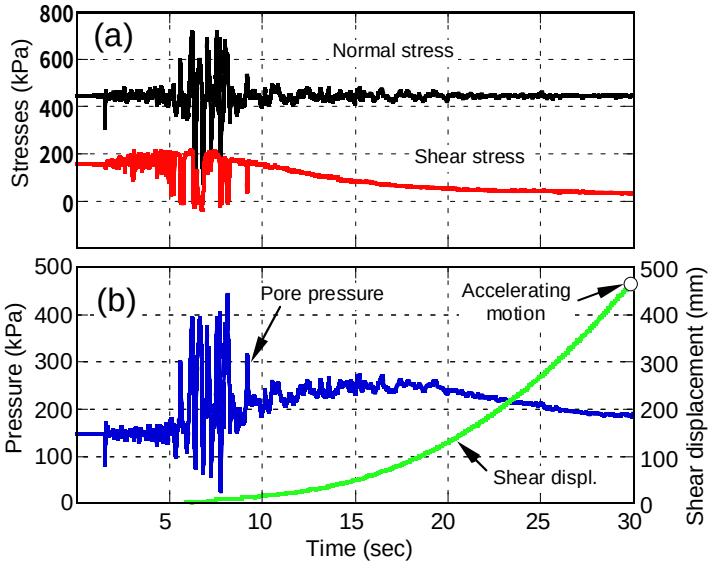

Fig. 31 Time series data for naturally drained cyclic test on saturated gravel layer (B_D = 0.99)

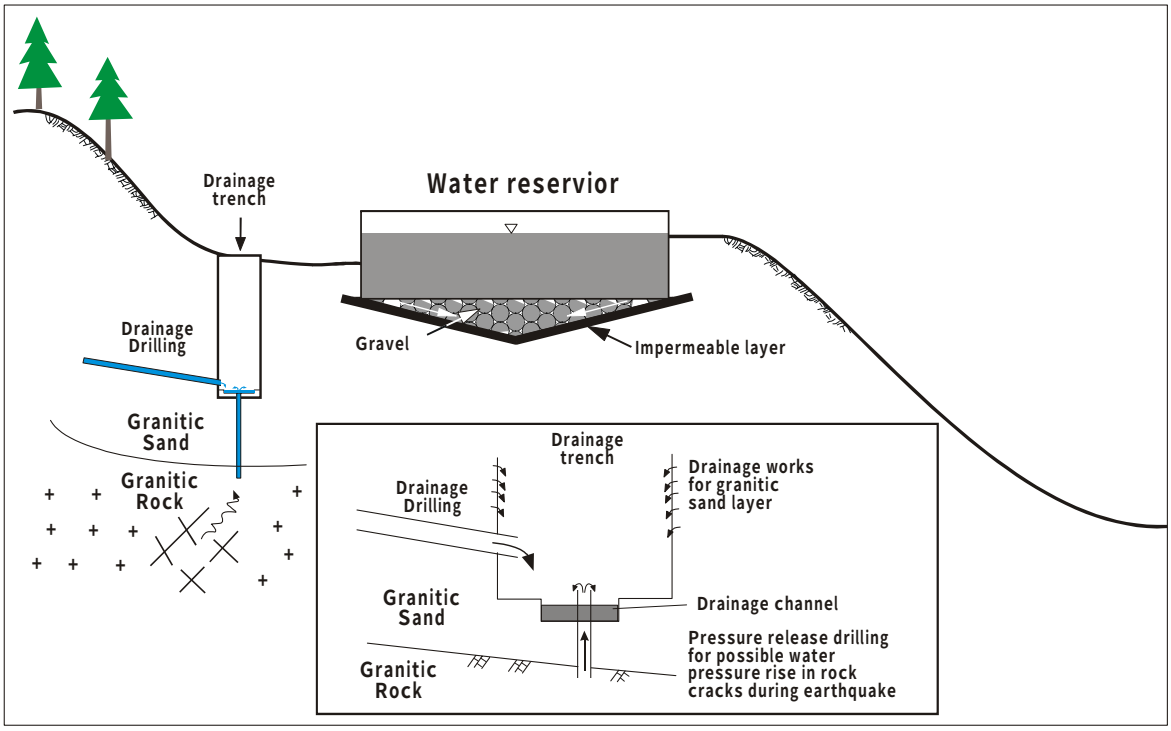

Fig. 32 Proposed measures for prevention of sliding surface liquefaction failure

5.2 A Densely Populated Urban Area Near Tokyo

The landslide risk assessment has also been performed on a densely populated urban area near Tokyo, as part of APERITIF Project. Fig. 33 gives an example of densely populated urban area near Tokyo. Fig. 34 presents the micro-contour map of this area. This map was made as a part of APERITIF project by the Geographical Survey Institute, Japan, using laser scanner-based topographic survey method, in which the effects of buildings and forests had been removed and the level of ground surface was presented in high resolution. In this figure, two kinds of landforms, i.e., concave valley landform (**A**: the previous landslide area) and convex mountain ridge landform (**B**), could be found on the boundary

between the residential grounds and the mountainous lands. Furthermore, from point **C** (on the downstream of point **B**), a river came out of the ground. Comparing to air photos taken before the land development, it is identified that a valley was filled until point **C**. In Fig. 34, the topographic feature of previous landslides could be recognized.

The area showing concave valley landform with higher capacity of ground water and surface water catchment may be dangerous during rainstorm. On the other hand, the mountainous ridge of area **B** can also be dangerous during earthquakes, if the recognized sandy aquifer on area **A** extends to the soil layers below the mountainous ridge of area **B**. In this case, high excess pore water pressure could be built up on the saturated sand layer during earthquakes. If the mountainous ridge of area B fails, and the landslide mass would ride on the (possibly) saturated soil layer of the valley fillings, a high pore pressure generation could be triggered on the valley fillings by the undrained loading due to the displaced soil mass from the mountainous ridge, and then rapid long travelling landsliding could be resulted in. In general, landslides on the urban areas are not so big; if the landslide risk has been clarified; the countermeasures are possible in existing technology. Therefore, reliable method for the assessment of landslide risk is very necessary and important.

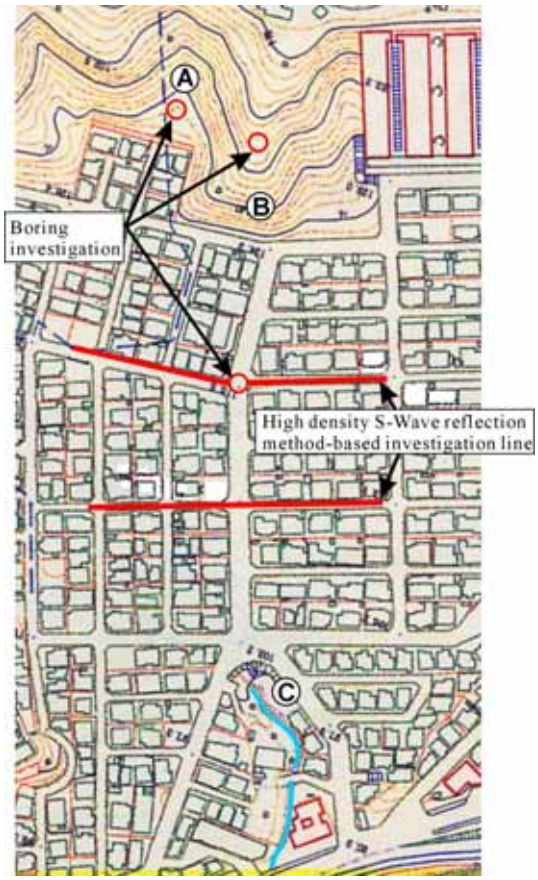

Fig. 33 A case of housing development area near Tokyo

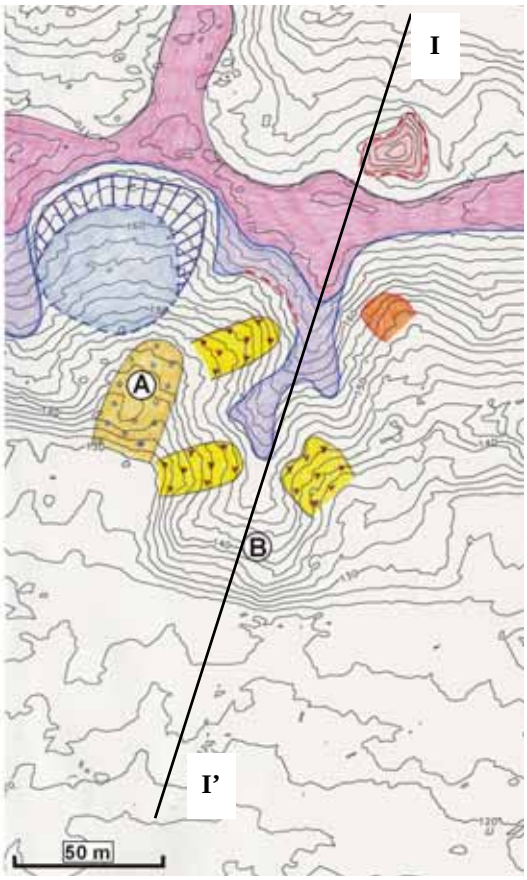

Fig. 34 Laser scanner-based micro-contour map of the housing development area (made by the Geographical Survey Institute, Japan)

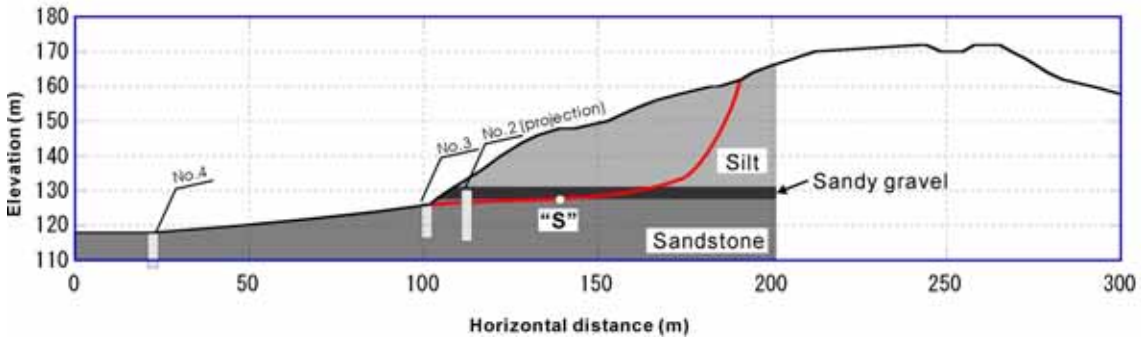

Fig. 35 Cross section along line I-I' in Fig. 34.

Boring investigation was also performed on this urban area, and samples for geotechnical testing were obtained from the boring cores. Fig. 35 presents a cross section along the I-I' line on Fig. 34, basing on the boring investigation. A potential sliding surface is inferred as shown in Fig. 35. To examine the properties of the soil layer along the potential sliding surface, undrained ring shear tests were conducted on these samples. Here the results of one test on the sample from the sandy layer are presented to give a preliminary understanding on the cyclic behaviour of the soil layer within the slope. When the potential sliding surface passes through the boundary between the gravel layer and sandy layer (point "S" in Fig. 35), it has an average inclination of 10 degrees, and the thickness of the overlaid soil layer reaches 20 m approximately.

Because the main purpose of the test was to examine and assess the possible landslide hazards on these area, undrained cyclic ring shear test was performed by applying a cyclic shear stress whose amplitude was kept increase with cycle, while the normal stress was kept constant (see Fig. 36a). The frequency was 1.0, and 10 cycles of cyclic shear loading were applied. According to the above-laid soil layer thickness and the slope angle, the initial normal stress and shear stress were calculated approximately as 380 and 61 kPa, respectively. After the samples were saturated and normally consolidated, the cyclic loading (Fig. 36a) was applied. The test results were presented in Fig. 36 in the form of time series data (Fig. 36b) and effective stress path (Fig. 36c). As revealed by the test results, shear failure was triggered within 5 cycles; accelerating shearing was resulted in even after the termination of cyclic loading, i.e., shear failure continued under the static shear stress due to the soil weight itself. The shear resistance reduced with progress of shearing to a very small value at the final steady state, showing a small apparent friction angle of 4.5 degrees. Although detailed analysis on this area is still on process, it could be concluded from the results of boring survey and laboratory investigation that this area is of high possibility to suffer rapid long travel landslide hazards during earthquake.

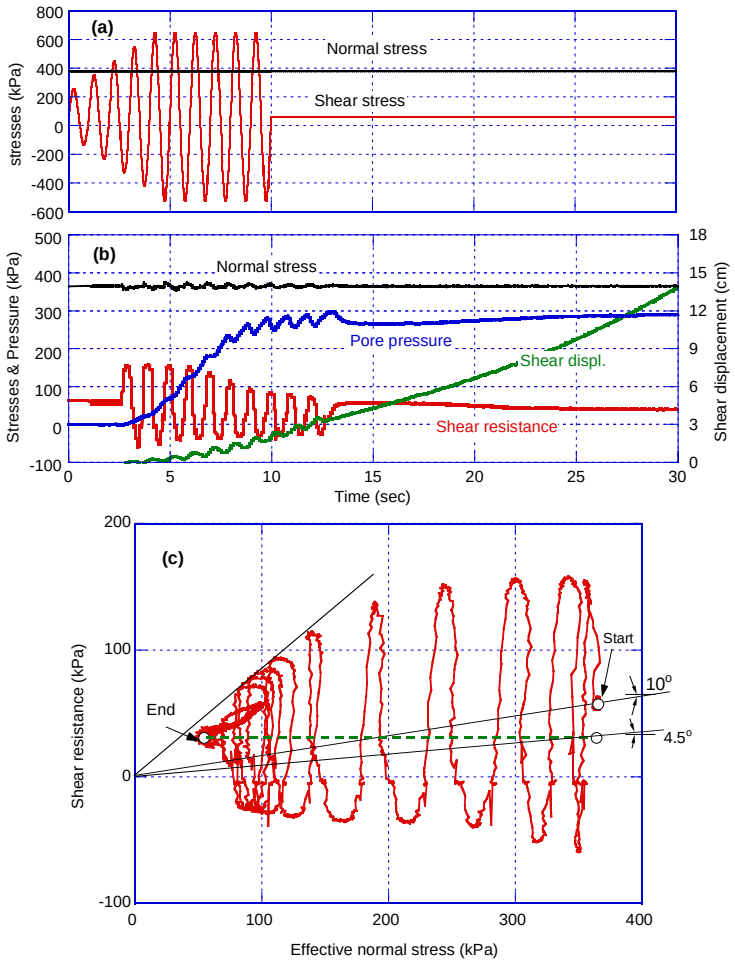

Fig. 36 Cyclic loading control signal for normal stress and shear stress (a), and the undrained cyclic ring shear test results in form of time series data (b) and effective stress path (c) (B_D = 0.98).

6. Conclusions

The conclusions could be made as follows:

(1) From well-documented and investigated examples of recent earthquake/rainfall-induced landslides in urban areas, the mechanisms of these catastrophic landslides were introduced in this paper.

(2) The ring shear geotechnical simulation test has been performed for several cases. The test results revealed that grain crushing of saturated granular material had a critical role for the mechanism of liquefaction in the shear zone. This phenomenon is called as sliding-surface liquefaction. This liquefaction will be caused with progress of shearing. Therefore, this is not conventional liquefaction-induced-landslide, but landslide-induced liquefaction. Liquefaction in the shear zone enables a landslide with high mobility.

(3) Undrained ring shear test to simulate the Nikawa landslide by loading normal stress and shear stress estimated from the monitored seismic records reproduced a shear failure and a low apparent friction angle of 6.3 degrees at steady state. The shear resistance continued to decrease with progress of shearing even after the stop of seismic loading.

(4) Field survey on the Tsukidate landslide revealed that sliding-surface liquefaction failure on the saturated shear zone of crushable pyroclastic fillings was the key reason for the rapid long travelling flow phenomenon on gentle slope.

(5) Application of the ring shear test to soils from the Minamata debris flow simulated a landslide triggered by the gradual increase of ground-water level during heavy rainfall. Sliding surface liquefaction resulted with the progress of shearing even in the naturally drained condition corresponding to the gradual increase of pore water pressure in the debris-flow materials. An undrained ring shear test was carried out simulating the undrained loading process that takes place in the pre-existing torrent deposits and the weathered surface soils on the valley slopes. This revealed that only a small increment in the shear stress due to the impacting by the displaced soil mass could have caused shear failure of these deposits/soils with the generation of high pore water pressure. In addition, the volume of the landslide mass was increased by entrainment of these deposits/soils.

(6) Basing on the knowledge acquired through those above-mentioned case studies, approaches for risk identification of catastrophic landslide disasters due to the sliding surface liquefaction for concerned locations in planning are proposed and applied for two urban areas in Japan.

(7) The assessment of landslide risk on the Nikawa slope area was performed on the bases of field investigation and laboratory ring shear simulation tests. Field investigation revealed that a possible shear failure could be resulted along a boundary of granitic gravel layer and sandy layer. The undrained ring shear test results showed that sliding surface liquefaction could be triggered in both the sandy layer and the gravel layer. The excess pore pressure was continued to build up after the main shock due to grain crushing with progress of shearing, although a certain of excess pore-water pressure was built up during the main shock of earthquake. The dissipation of generated pore pressure from the shear zone is essential to the motion of displaced landslide mass. As revealed by the naturally drained ring shear test results, gravel layer including silts could suffer failure with long traveling displacement due to its low permeability. Therefore, more attention should be paid to preventing the possible liquefaction failure of the gravel layer during earthquakes on this site.

(8) The assessment of landslide risk on a densely populated urban area near Tokyo has also been planed and performed. Detailed laser scanner-based micro-contour mapping, geological and geotechnical consideration revealed that this area is also facing the risk of rapid long traveling landslides during rainstorm or earthquake. Detailed researches, including the geological features as well as the mechanical behavior of gully-burry fills are in progress.

Acknowledgements

Support by the Japanese Ministry of Education, Culture, Sports, Science and Technology (MEXT) 21st Century COE Program for DPRI, Kyoto University (No. 14219301, Program Leader: Prof. Yoshiaki Kawata) is appreciated. This research was also supported by the project, "Areal Prediction of Earthquake and Rain Induced Rapid and Long-travelling Flow Phenomena" (APERIF), of the Special Coordinating Fund for Promoting Science and Technology of the Ministry of Education, Culture, Sports, Science and Technology of Japan (MEXT) (Project Leader: Prof. Kyoji Sassa). The real seismic record at the JR Takarazuka Station was provided by Japan Railway Technical Research Institute. The assessment of landslide risk on Nikawa slope area was conducted cooperatively with Nippon Koei Co., Ltd.

References

Fukuoka, H., Wang, G., Sassa, K., Wang, F., and Matsumoto, T. (2004): Earthquake-induced rapid long-travelling flow phenomenon: the case of May 2003 Tsukidate landslide in Japan. *Landslides* (in contribution).

Fukushima, Y., Tanaka, T. (1990): A new attenuation relation for peak horizontal acceleration of strong earthquake ground motion in Japan, *Bulletin of the Seismological Society of America*, Vol. 80 (4), pp. 757-783.

Geographical Survey Institute, Japan (1996): *Active fault map in urban area: Northwest part of Osaka*.

Irikura, K. (1996): Strong ground motion of the Hyogoken-Nanbu earthquake and the fault model, *The Great Hanshin-Awaji Earthquake Disaster for the Disaster Prevention Research*, DPRI, Kyoto University, pp. 81-98 (in Japanese).

Sassa, K. (1996): Prediction of earthquake induced landslides, *Proceedings of 7th International Symposium on Landslides*, A.A. Balkema, Rotterdam, The Netherlands, 1, pp115-132.

Sassa, K., Fukuoka, H., Scarascia-Mugnozza, G., Evans, S. (1996): Earthquake-induced-landslides: Distribution, motion and mechanisms, *Soils and Foundations*, Special Issue, pp53-64.

Sassa K. (1995): Access to the dynamics of landslides during earthquakes by a new cyclic loading ring shear apparatus, *Proc. for 6th International Symposium on Landslides*, *Landslides*, Balkema, Rotterdam, Vol. 1, pp. 1919-1939.

Sassa, K., Wang, G., and Fukuoka H. (2003): Performing undrained shear tests on saturated sands in a new intelligent type of ring shear apparatus", *Geotechnical Testing Journal*, 26(3), pp. 257-265.

Sassa, K., Fukuoka, H., Wang, G., and Ishikawa, H. (2004): Undrained dynamic-loading ring-shear apparatus and its application to landslide dynamics, *Landslides*, Vol. 1(1), pp. 7-19.

Wang, G., Sassa, K. (2002): Post-failure mobility of saturated sands in undrained load-controlled ring shear tests, *Canadian Geotechnical Journal*, 39(4), pp. 821-837.

Wang G, Sassa K, Fukuoka H (2003) Downslope volume enlargement of a debris slide-debris flow in the 1999 Hiroshima, Japan, rainstorm. *Engineering Geology*, Vol. 69, pp. 309-330.

Sassa K, Fukuoka H, Wang FW (1997) Mechanism and risk assessment of landslide- triggered-debris flows: lesson from the 1996.12.6 Otari debris flow disaster, Nagano, Japan. D.M. Cruden & R. Fell, eds. *Landslide Risk Assessment*, Proceedings of the international workshop on landslide risk assessment. Honolulu, 19-21 February, pp. 347-356.

要　旨

近年日本の都市域において地震･降雨により発生した以下の三箇所の地すべりを紹介した。(1) 1995 年兵庫県南部地震により 20 ° の緩斜面で発生し、34 人の犠牲が出た仁川地すべり、(2) 2003 年 5 月の三陸南地震により、平均傾斜が約 10 度の緩斜面で発生した宮城県築館町の地すべり、(3) 2003 年 7 月の豪雨により熊本県水俣市宝川内地区で発生した土砂災害。現地で採集した土試料に対し、非排水リングせん断試験を実施し、上記の地すべりの発生･運動メカニズムについて検討した。その結果、すべり面液状化がこの三つのケースにおける高速長距離運動の最も重要な因子であることが立証された。この結果に基づいて、すべり面液状化を考慮した都市域地すべり危険度を評価する方法を提案した。さらに、この方法を用いて仁川地区と首都圏のある住宅密集地において地震時斜面災害の予測を試みた。仁川地区に対する詳しい地質調査と地震時地すべり再現試験結果により、仮に 1995 年兵庫県南部地震と同じ震度の地震が再び西宮市仁川地区を襲った場合、仁川地すべりの上方隣接斜面内にすべり面液状化が発生しうる土層があることを見出した。試験結果により、予め地下水位を下げておくことにより、主要動直後に発生する過剰間隙水圧下でもこの土層の変動を抑止することができ、すべり面液状化を防げることがわかり、対策工法として提案した。また、レーザースキャナーによる高精度地すべり地形の判読、地質調査、及び非排水リングせん断試験に基づいた総合解析により、首都圏の住宅密集地の尾根型斜面において、地震時高速長距離土砂流動現象が発生しうることが分かった。

キーワード: 地すべり, 地震, 降雨, 液状化, 危険度評価, 都市域